Modelling The First Probable Two Plane Lens System B2114+022: Reproducing Two Compact Radio Cores A, D

Kyu-Hyun Chae,[1] Shude Mao,[1] Pedro Augusto[2]

[1] *University of Manchester, Jodrell Bank Observatory, Macclesfield, Cheshire SK11 9DL, UK*
[2] *Universidade da Madeira, Dep. Matemática, Caminho da Penteada, 9050 Funchal, Portugal*

ABSTRACT

We test possible lensing scenarios of the JVAS system B2114+022, in which two galaxies at different redshifts ("G1" at $z_1 = 0.3157$ and "G2" at $z_2 = 0.5883$) are found within 2 arcseconds of quadruple radio sources. For our investigation, we use possible lensing constraints derived from a wealth of data on the radio sources obtained with VLA, MERLIN, VLBA and EVN as well as HST imaging data on the two galaxies, which are presented in Augusto et al. In the present study, we focus on reproducing the widest separated, observationally similar radio components A and D as lensed images. We first treat G2 (which is the more distant one from the geometric centre) as a shear term, and then consider two plane lensing explicitly including G2's potential at the z_2 plane as the first case of two plane lens modelling. Our modelling results not only support the hypothesis that the system includes gravitationally lensed images of a higher redshift extragalactic object, but they also show that the explicit inclusion of G2's potential at the second lens plane is necessary in order to fit the data with astrophysically plausible galaxy parameters. Finally, we illustrate a natural consequence of a two-plane lens system, namely the prediction of distortion as well as shift and stretching of G2's isophotes by G1's potential, which can in principle be measured by subtracting out G1's light distribution in a high S/N and good angular resolution image, especially a multi-colour one.

Key words: gravitational lensing - cosmology: theory - dark matter - galaxies: structure

1 INTRODUCTION

At the time of writing (December 2000), there are ~ 60 confirmed or candidate multiply-imaged extragalactic sources. All these systems except possibly for B2114+022 appear to have lensing object(s) at a single redshift, although various astrophysical perturbations may exist at different redshifts (Keeton, Kochanek & Seljak 1997). The lens candidate system B2114+022 was found by Augusto et al. (2000; hereafter A00) as the sixth strong lens candidate in the Jodrell-VLA Astrometric Survey (JVAS) which along with the follow-up Cosmic Lens All Sky Survey (CLASS) discovered 19 new lenses or lens candidates (e.g. Browne 2000). The field of the JVAS system B2114+022 includes two early type galaxies at different redshifts ($z = 0.3157$ and 0.5883) separated by $\approx 1''.3$, and four radio sources two of which are separated by $\approx 2''.6$ enclosing the two galaxies within the diameter. These two widest separated components (A and D) have similar radio imaging and spectral properties and are most likely to be lensed images, while the other two components are open to several alternative astrophysical origins possibly including lensing, based upon presently available data (see A00). In this paper, we consider a realistic two plane lens model for B2114+022 A, D.

The basic equations of multiple plane lensing are well known, and can be derived elegantly from Fermat's principle (Blandford & Narayan 1986; Kovner 1987). In general, the properties of multiple plane lensing are much more complicated than those of single plane lensing, although some single-plane theories remain valid in the case of multiple plane lenses (Seitz & Schneider 1992). Due in part to this complexity, only relatively simple two-plane deflectors have been studied so far. Erdl & Schneider (1993) gave a complete classification of the critical curves and caustics for two point lenses distributed in different planes, while Kochanek & Apostolakis (1988) investigated the lensing properties of two spherical deflectors at different redshifts. The properties of two plane lensing by elliptical deflectors (e.g. caustic properties) are essentially unknown. This paper is in part an investigation of the properties of two plane lensing by elliptical deflectors as example models of B2114+022.

Kochanek & Apostolakis (1988), using the above model,

predicts that 1–10 per cent of gravitational lenses should be two plane lenses. This theoretical prediction is broadly consistent with the statistics of the well-defined, complete CLASS survey, i.e. one two-plane lens candidate out of 19. The fact that no additional two plane lens was discovered in the rest of ~ 40 more heterogeneous lenses hints that other (less well-defined) surveys may be biased against the discovery of multiple plane lenses. Nevertheless, as the number of observed lenses increases rapidly, we expect that more two plane lenses will be discovered in the future allowing us to use them for astrophysical applications (e.g. galactic structures and evolution, constraining cosmological parameters).

This paper is organized as follows. In section 2, we briefly review the theory of two plane lensing and summarize the equations. In section 3, we investigate possible lens models of B2114+022 A, D, with particular emphasis on the differences between the properties of a single-plane lens model and a two-plane lens model. In section 4, we discuss our results and point out directions for future work.

2   REVIEW OF TWO PLANE LENSING

In this section, we review the theory of two plane lensing. For further review, the reader is referred to the monograph by Schneider, Ehlers & Falco (1992).

Let $\vec{\xi}_1$, $\vec{\xi}_2$ and $\vec{\eta}$ be the physical vectors from a fiducial perpendicular line on the foreground lens, background lens and source planes, respectively (Figure 1). The fiducial line, called the optical axis, is defined in this paper as the line passing through the mass centre of the foreground deflector (Figure 1). Let $\hat{\alpha}_i(\vec{\xi}_i)$ $(i = 1, 2)$ be the deflection angles due to the foreground and background deflectors respectively. The impact vector $(\vec{\xi}_1)$ on the foreground lens plane is related to the physical source vector $(\vec{\eta})$ and the impact vector $(\vec{\xi}_2)$ on the background lens plane by the following two plane and single plane lens equations:

$$\vec{\eta} = \frac{D_s}{D_1}\vec{\xi}_1 - D_{1s}\hat{\alpha}_1(\vec{\xi}_1) - D_{2s}\hat{\alpha}_2(\vec{\xi}_2) \qquad (1)$$

and

$$\vec{\xi}_2 = \frac{D_2}{D_1}\vec{\xi}_1 - D_{12}\hat{\alpha}_1(\vec{\xi}_1). \qquad (2)$$

In the above all the distances are angular diameter distances. As for the single plane lens case, it is convenient to re-scale the physical vectors by length units in proportion to the angular diameter distances to the three planes from the observer, i.e., by ξ_0 (an arbitrary length), $\xi_0 D_2/D_1$ and $\xi_0 D_s/D_1$; in other words, we define $\vec{x}_1 \equiv \vec{\xi}_1/\xi_0$, $\vec{x}_2 \equiv \vec{\xi}_2/(\xi_0 D_2/D_1)$ and $\vec{x}_s \equiv \vec{\eta}/(\xi_0 D_s/D_1)$ (e.g. for $\xi_0 = D_1$, they become angle vectors). Using these dimensionless scaled quantities, the lens equations (1) and (2) become

$$\vec{x}_s = \vec{x}_1 - \vec{\alpha}_1(\vec{x}_1) - \vec{\alpha}_2(\vec{x}_2) \qquad (3)$$

and

$$\vec{x}_2 = \vec{x}_1 - \beta_{12}\vec{\alpha}_1(\vec{x}_1), \qquad (4)$$

where

$$\vec{\alpha}_i(\vec{x}_i) = \nabla\psi_i(\vec{x}_i) \qquad (i = 1, 2) \qquad (5)$$

are scaled dimensionless deflection angles, and

$$\beta_{12} = \frac{D_{12}D_s}{D_2 D_{1s}}. \qquad (6)$$

In equation (5) the dimensionless potentials are given by

$$\psi_i(\vec{x}_i) = \frac{1}{\pi}\int d^2x' \kappa_i(\vec{x}_i)\ln|\vec{x}_i - \vec{x}'| \qquad (i = 1, 2) \qquad (7)$$

where

$$\kappa_i(\vec{x}_i) \equiv \frac{\Sigma_i(\xi_i\vec{x}')}{\Sigma_{\text{cr},i}} \qquad (i = 1, 2). \qquad (8)$$

Here $\Sigma_i(\xi_i\vec{x}')$ are physical surface mass densities, and $\Sigma_{\text{cr},i}$ are critical surface mass densities defined by

$$\Sigma_{\text{cr},i}^{-1} \equiv \frac{4\pi G}{c^2}\frac{D_i D_{is}}{D_s}, \qquad (9)$$

similarly to the single plane lens case.

The inverse magnification matrix $[\mathcal{M}^{-1}]$ of lensing is found from equations (3) and (4) to be

$$
\begin{aligned}
[\mathcal{M}^{-1}] &= \left[\frac{\partial\vec{x}_s}{\partial\vec{x}_1}\right] \\
&= \mathcal{I} - \begin{bmatrix} \psi_{1,xx} & \psi_{1,xy} \\ \psi_{1,yx} & \psi_{1,yy} \end{bmatrix} - \begin{bmatrix} \psi_{2,xx} & \psi_{2,xy} \\ \psi_{2,yx} & \psi_{2,yy} \end{bmatrix} \\
&\quad + \beta_{12}\begin{bmatrix} \psi_{1,xx} & \psi_{1,xy} \\ \psi_{1,yx} & \psi_{1,yy} \end{bmatrix}\begin{bmatrix} \psi_{2,xx} & \psi_{2,xy} \\ \psi_{2,yx} & \psi_{2,yy} \end{bmatrix},
\end{aligned}(10)
$$

where $\mathcal{I}$ is a unit matrix. Equation (10) has a cross term proportional to the distance between the two lens planes which would not exist for lensing by two deflectors in the same lens plane.

The time delay for the light ray following a deflected light path relative to the undeflected path from the source to the observer is given by the sum of delays for the two planes, i.e.,

$$
\begin{aligned}
t &= \frac{1+z_1}{c}\frac{\xi_0^2 D_2}{D_1 D_{12}}\left[\frac{1}{2}(\vec{x}_1 - \vec{x}_2)^2 - \beta_{12}\psi_1(\vec{x}_1)\right] \\
&\quad + \frac{1+z_2}{c}\frac{\xi_0^2 D_2 D_s}{D_1^2 D_{2s}}\left[\frac{1}{2}(\vec{x}_2 - \vec{x}_s)^2 - \psi_2(\vec{x}_2)\right], \qquad (11)
\end{aligned}
$$

where z_1 and z_2 are, respectively, the redshifts of the foreground and background deflectors.

3   APPLICATION TO B2114+022

3.1   Observed Properties of B2114+022

A full description of observed properties of B2114+022 is given in A00. Below we only summarize the main properties and the observational constraints to be used in lens modelling. A field of B2114+022 can be found in Figure 2, which shows the geometric arrangements of the radio components and the galaxies based on present absolute and relative astrometries (Table 4, A00).

3.1.1   Radio Sources in a Unique Configuration

B2114+022 is one of few JVAS/CLASS systems whose astrophysical origins have not been well understood to date. As shown in Figure 2, there are four radio sources located within $\approx 2\rlap{.}''6$ of each other. The widest separated components A and D in B2114+022 are similar in their radio properties;
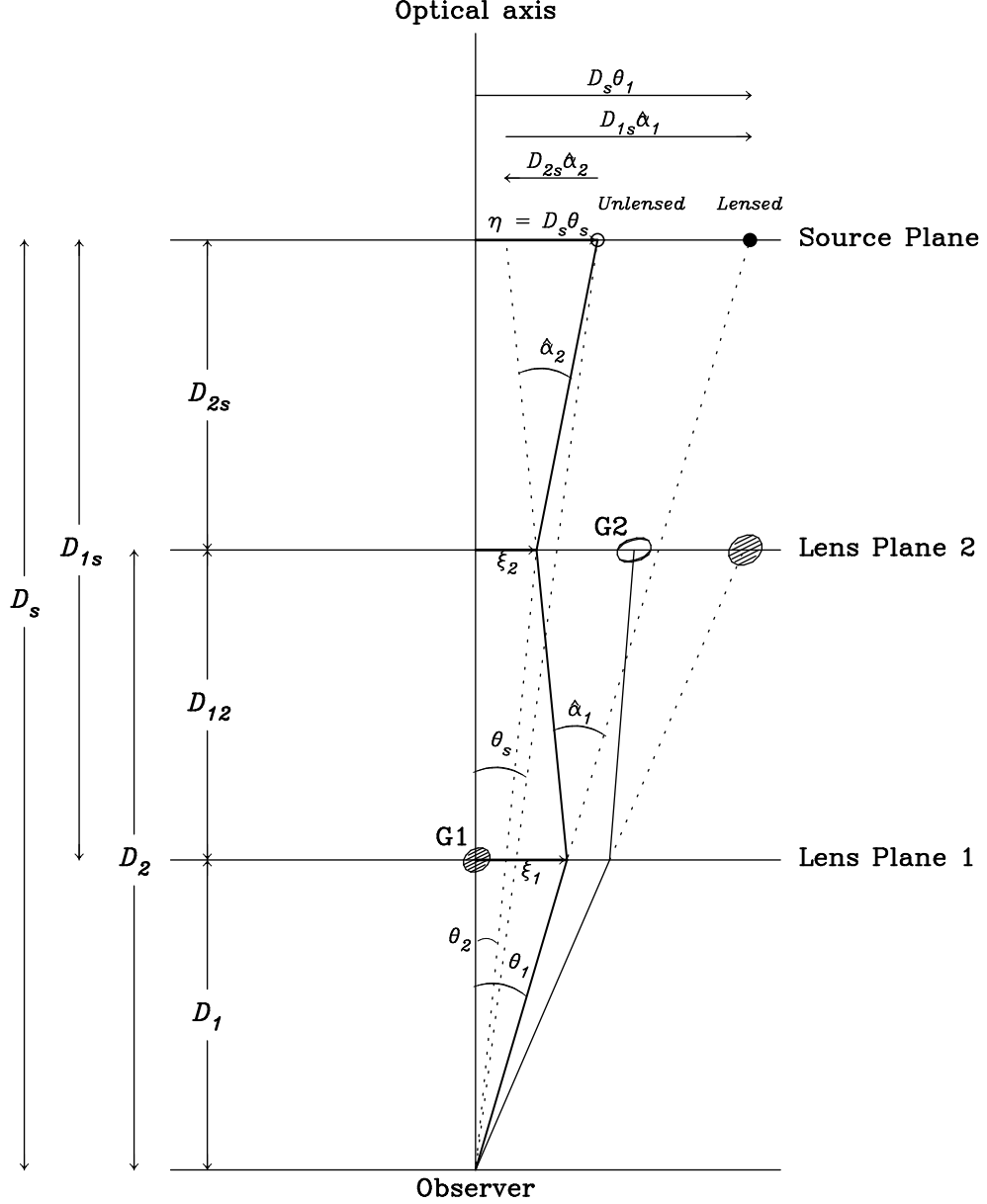
Figure 1. Source and image positions and ray-paths for two plane lensing. The physical quantities used in section 2 are indicated. The shift of the background lens's position due to the foreground lens is illustrated. Although not shown in the diagram, isophotes of the background galaxy are stretched and distorted resulting in apparent change in the galaxy's position angle, ellipticity and isophotal shapes.

they are both compact and have similar radio spectra over a frequency range from $\nu = 1.5$–15 GHz, while the other two components found close to G1's optical centre and component A are more resolved and have spectral peaks at higher frequencies (Figures 2 and 3, A00). Two optical galaxies (see section 3.1.2) are found in the field with components A, B and C at the same side while only component D is at the opposite side.

The geometric arrangements of the galaxies with respect to the radio components and the radio imaging and

spectral similarities between components A and D hint that components A and D may be counter images of a higher redshift radio source lensed by the potentials of the galaxies. Based solely on the geometry of the system, it would be possible that three or all four radio components are lensed images of the same source. In such scenarios, however, the different radio imaging and spectral properties of components B and C compared to those of components A and D need to be explained via modifications of images through the passage of the galactic media of G1. Since such an ex-
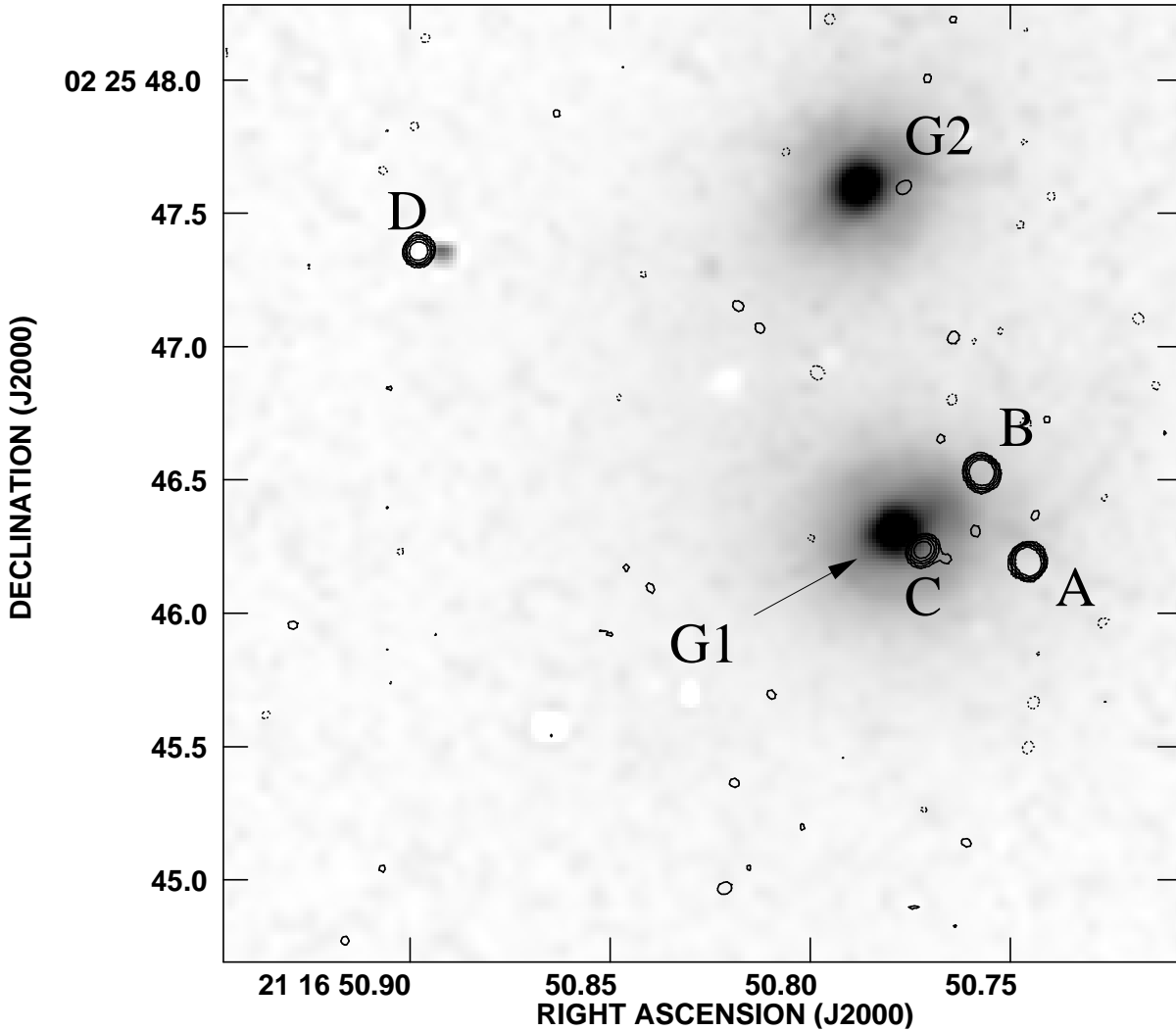
Figure 2. The observed geometric arrangement of the radio sources with respect to the two optical galaxies in B2114+022 (reproduced from A00).

planation lacks observational evidence at present, modelling components B and C as lensed images is not motivated (at present); it will, however, be worthwhile to revisit the issue in the future with better radio data and/or alternative interpretations of the present data (see section 4). The lensing hypothesis for components A and D is further supported using the following simple lensing analysis. If the unknown redshift of component A is somewhat higher than that of G1 ($z_1 = 0.3157$) and G1 has a moderate velocity dispersion, it is required that component A has counter image(s) because its impact parameter from G1's centre is smaller than an Einstein ring radius using a singular isothermal sphere

(SIS) model for G1. For example, for a source redshift $z_s \gtrsim 1$ and a line-of-sight velocity dispersion $\sigma_v \gtrsim 185$ km s^{-1}, an SIS Einstein ring radius is larger than the impact parameter of component A at G1 ($\approx 0.''56$). However, the flux ratio between components A and D is uncommon in single-plane double lenses, namely that component A (which is closer to G1) is ≈ 3 times brighter. This unusual flux ratio between components A and D should then be attributed to the combined effect of the two galaxies found in the field if they are lensed images.

Unlike components A and D, components B and C are difficult to interpret in several ways (see A00 for further dis-

Table 1. Relative positions of radio and optical sources and radio flux density ratios. Observations used are as follows. (1) Radio component positions: MERLIN 1.6 GHz, VLBA 5.0 GHz, MERLIN+EVN 1.6 GHz. (2) Radio component flux density ratios: VLA 8.4 GHz, 15 GHz, MERLIN 5 GHz. (3) Relative positions of G1 with respect to radio component A: NOT I band + VLA 8.4 GHz. (4) Relative positions of G2 with respect to G1: NICMOS H band.

Component	$\Delta\alpha$ (arcsec)	$\Delta\delta$ (arcsec)	R_{f_ν}
A	$\equiv 0$	$\equiv 0$	$\equiv 1$
B	0.175 ± 0.001	0.333 ± 0.001	0.90 ± 0.03
C	0.397 ± 0.001	0.043 ± 0.001	0.28 ± 0.02
D	2.286 ± 0.001	1.158 ± 0.002	0.32 ± 0.02
G1	0.555 ± 0.1	0.04 ± 0.1	—
G2	0.145 ± 0.006 [a]	1.296 ± 0.006 [a]	—

[a] Relative positions of G2 with respect to G1

cussion). First, components B and C are at the same side of G1 (with a 3σ astrometric significance), which is difficult to reconcile with a possibility that they are double radio ejections from G1. Second, they have more extended image structures while their spectra peak at higher frequencies compared with the more compact components A and D. Finally, both components B and C are within $0''.5$ of G1, which is smaller than an Einstein ring radius of G1 for a moderate velocity dispersion of G1 and an intermediate source redshift (see above), and the angular separation between components B and C is $0''.36$, which is 7 times smaller than the separation between components A and D, i.e. $2''.56$. This last point from the geometry of B2114+022 virtually rules out a possibility that components B and C are lensed images of an independent source due to the same potentials which are supposed to give rise to components A and D, although it would not be inconsistent with a possibility that they are counter images of components A and D.

Deep HST optical/near infrared observations of B2114+022 have not resulted in any detection of optical counterparts of the radio components down to $I = 25$ (WFPC2, F814W) and $H = 23$ (NICMOS, F160W). This may not be surprising for components B and C because of their proximity to G1's centre. The apparent extreme faintness of components A and D at optical wavelengths may indicate that their source is a high redshift and/or an intrinsically faint object, such as a low luminosity radio galaxy.

Table 1 summarizes A00's relative positions of radio components B, C and D and the two galaxies with respect to component A, and the flux density ratios of the radio components. These flux density ratios do not include A00's 1.6 GHz data (Table 3 of A00), at which the spectra of components B and C are already turned over while those of components A and D start to turn over (see Figure 3 of A00). The flux ratio of D/A most relevant for this study is not significantly affected if 1.6 GHz data are included.

3.1.2 Two Close Galaxies with Different Redshifts

The two galaxies found close to the radio components have different redshifts, namely $z_1 = 0.3157$ for G1 and $z_2 = 0.5883$ for G2, making them the first possible two plane lens. G1 is nearly on the line joining components A and D while G2 is misaligned with the line. Within the framework of single plane lensing, this would seem to suggest that G1 is responsible for most of the lensing while G2 provides only a second-order effect in a lensing hypothesis. However, this is not quite so for two reasons. First, the observed position of G2 is a deflected position due to G1. Second, light rays from the source were deflected by G2 before they were deflected by G1 finally forming the observed images. In fact, the undeflected source position can be closer to (the undeflected) G2 than G1 in a reasonable two plane lens model (section 3.2.2 and Figure 6).

HST WFPC2 V (F555W) and I (F814W) band and NICMOS H (F160W) band observations of the galaxies reveal that both galaxies are moderately elliptical with fitted ellipticities and position angles somewhat fluctuating as a function of semi-major axis (see Figure 3). Application of a K-correction to A00's measured magnitudes of G1 and G2 in the above wave-bands, by assuming $S_\nu \sim \nu^{-2}$, gives an estimate of the apparent luminosity ratio of $L(\text{G2})/L(\text{G1}) \sim 3$ (N. Jackson; personal communication). However, since G2's apparent luminosity was magnified due to G1's potential, we estimate a true luminosity ratio of $L(\text{G2})/L(\text{G1}) \sim 2$ after correcting for a magnification of ~ 1.4 for G2 (see Figure 5). For similar mass-to-light ratios for the two galaxies, this luminosity ratio would imply that G2 is more massive than G1.

3.2 Lens Modelling

In this section we investigate possible lens models of B2114+022. One goal of doing so is to test lensing hypotheses for this system, in particular the possibility of reproducing components A and D using an astrophysically plausible model. If one can find a successful lens model, the lensing hypothesis will be strengthened. This is particularly important for this system since optical spectroscopy of the radio components appears to be extremely difficult due to extreme faintness of the radio sources at optical wavelengths and relatively large contamination from the galaxies (see section 3.1.1). Another goal is to study two plane lensing, particularly by making comparisons of the lensing properties of single plane lens models and two plane lens models for B2114+022.

In section 3.2.1, we first consider a popular single plane lens model, namely a power-law ellipsoid plus a shear, in which the shear term is intended to account for the lensing effect due to G2. In section 3.2.2, we consider two plane lensing by explicitly including G2's potential at the observed redshift. For each galaxy, we adopt a power-law mass model which includes an isothermal model as a special case, i.e., surface mass density of the form,

$$\Sigma(\xi, \theta) = \frac{\Sigma_0}{\left\{ 1 + \left(\frac{\xi}{\xi_c}\right)^2 [1 + e\cos 2(\theta - \theta_0)] \right\}^{(\nu-1)/2}}, \qquad (12)$$

where $\nu = 2$ corresponds to an isothermal radial index, $\xi \equiv \sqrt{\xi_x^2 + \xi_y^2}$, parameter $e(> 0)$ is related to the ellipticity via $\epsilon = 1 - \frac{\xi_{min}}{\xi_{max}} = 1 - \sqrt{\frac{1-e}{1+e}}$, θ_0 is the standard position angle (P.A., north through east), and ξ_c is a core radius. We calculate lens models in a cosmology with $\Omega_m = 1$, $\Omega_\Lambda = 0$, and $H_0 = 60h_{60}$ km s^{-1} Mpc^{-1}. In this cosmology, one arcsecond corresponds to $4.7h_{60}^{-1}$ kpc and $6.3h_{60}^{-1}$ kpc on the
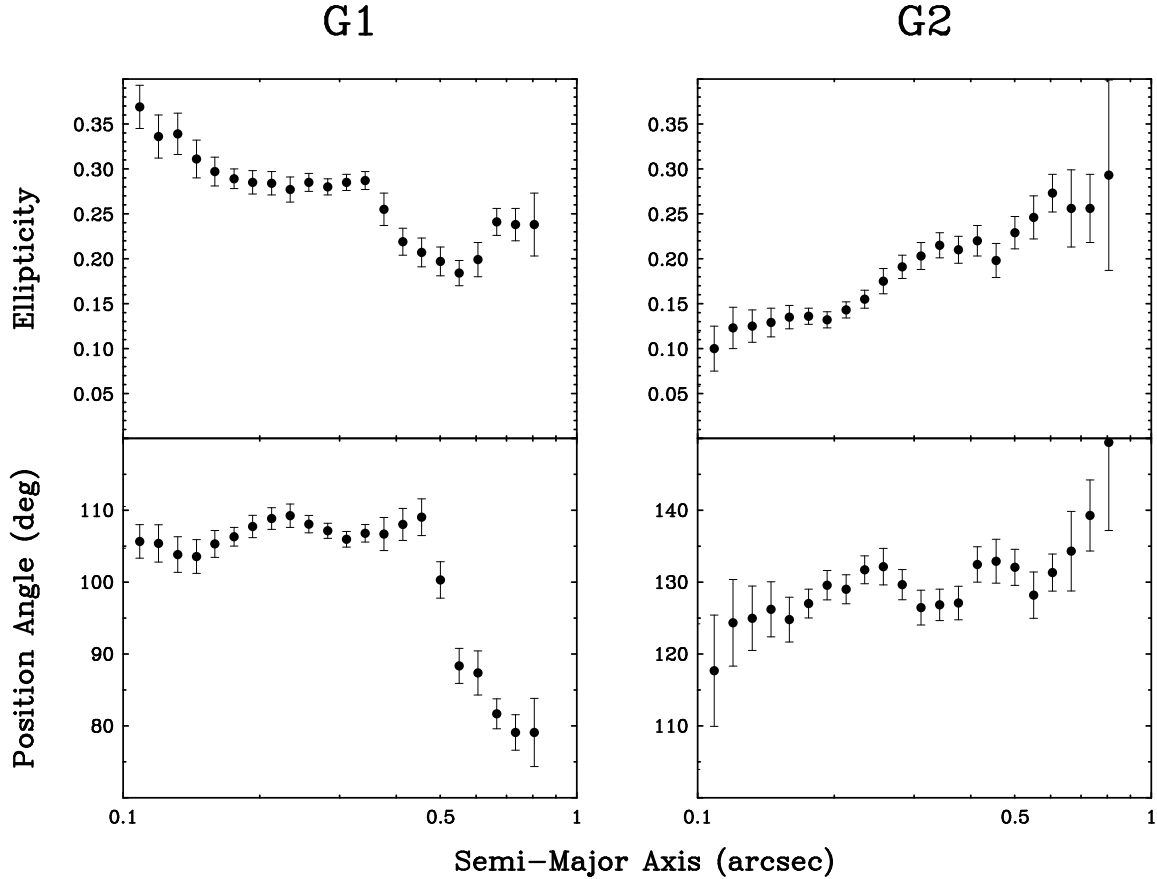
Figure 3. Ellipticity and position angle as a function of semi-major axis (in arcseconds) for the foreground (G1) and background (G2) galaxies derived from HST WFPC2 I band (F814W) images of the galaxies.

foreground and background lens planes respectively. Model parameters and predictions are dependent on the unknown source redshift (z_s) especially for $z_s \lesssim 1.5$; however, for $z_s \gtrsim 2$, the dependence is little. All parameters and predictions given below are for $z_s = 3$.

As was pointed out in section 3.1.1, components A and D would be consistent with a lensing hypothesis while the origin of components B and C is not obvious, at best. We thus use the observed positions of components A and D and their flux ratio as model constraints in this study. For a single plane lens model, G1's positions provide two additional constraints, while for a two-plane lens model, both galaxies provide four additional constraints. In total, there are 5 and 7 (direct) constraints for the single-plane and two-plane lensing cases, respectively.

The small number of constraints is a major difficulty in investigating lens models for B2114+022. For example, a mass model of the form given by equation (12) with fixed radial index and core radius even without a shear term has as many free parameters (i.e. ϵ, θ_0, Σ_0, and the two coordinates of the source on the source plane) as observational constraints. Fortunately, however, there are additional pieces of information on the galaxies from HST imaging which could

not be quantitatively used in lens modelling, nevertheless can provide crucial tests of lens models as regards astrophysical plausibility. For this purpose, the observed position angles and ellipticities and inferred luminosity ratio of the galaxies are (or can be) useful. First of all, a mass distribution significantly misaligned with the observed light distribution is unlikely since the study of an ensemble of gravitational lenses shows a general trend that the inferred mass distributions are aligned with the observed light distributions within $\sim 10°$ (Keeton, Kochanek & Falco 1999) at least for the lensing galaxies which are relatively isolated or in low density environments. Analyses of X-ray isophotes of three isolated early-type galaxies NGC 720, 1332 and 3923 [see the review by Buote & Canizares (1997) and references therein] show the general alignment between the mass and light, except that in NGC 720, for outer parts of the galaxy ($> R_e$) the mass and light are misaligned by $\sim 30°$. Analyses of the kinematics of polar rings in polar-ring galaxies also find the general alignment between the mass and light (Arnaboldi et al. 1993, Sackett et al. 1994, Sackett & Pogge 1995). Second, while the shape of dark matter distribution in galaxies is poorly known at present (see the review by Sackett 1999), the above X-ray studies by Buote & Canizares (1997) report

that the inferred mass ellipticities are similar to or somewhat higher than the observed optical light ellipticities. The individual modelling of lensing galaxies by Keeton et al. (1999) does not find any clear correlation between the light and inferred mass ellipticities; mass ellipticities are higher than light ellipticities for some lensing galaxies while it is the opposite for others. Given the present limited knowledge of the dark matter shape in galaxies, the observed light ellipticities of G1 and G2 can only provide a very limited test of lens models. For example, a disk-like mass shape for either G1 or G2 is unlikely given that the observed light distributions are only moderately elliptical. Finally, the luminosity ratio of the two galaxies can provide some information on the mass ratio of the two galaxies.

3.2.1 Test of Single Plane Lens Model: Ellipsoid plus Shear

To model B2114+022 with a single-plane lens, we need to incorporate G2's lensing effect, which to first order, can be modeled as a shear term. Its deflection is given by

$$\vec{\alpha}_\gamma(\vec{x}) = \gamma \begin{pmatrix} \cos 2\theta_\gamma & \sin 2\theta_\gamma \\ \sin 2\theta_\gamma & -\cos 2\theta_\gamma \end{pmatrix} \vec{x}, \qquad (13)$$

where γ and θ_γ are the shear strength and P.A. respectively. Since the shear term is intended to account for G2's lensing effect, we expect that the shear points to G2's direction from G1,[★] which roughly corresponds to $\theta_\gamma \sim 0°$. A shear oriented in a direction significantly different from this presumed direction would be difficult to interpret within the framework of single plane lensing. We thus fix $\theta_\gamma = 0°$ and investigate the effect of positive shear strength on the fitted galaxy parameter values.

Although we expect that a non-zero shear is necessary to fit the data (i.e. the relative positions of G1 and component D with respect to component A and the flux ratio between components A and D) with more suitable parameter values, we first consider a zero shear case to merely keep records of the determined parameter values to be compared with those for the non-zero shear case below. We find that for the isothermal ($\nu = 2$) galaxy profile, the data can be perfectly fit provided that $\epsilon = 0.77$ and $\theta_0 = 146°$. For a somewhat shallower profile of $\nu = 1.75$ (a profile shallower than this is excluded since a theoretical image near the mass centre becomes brighter than a 5σ radio flux limit on any unobserved image, i.e., 2.4% of component D's flux; Norbury et al. 2000), the required ellipticity is reduced to $\epsilon = 0.58$. For this zero (external) shear case of the single plane lens model, the required ellipticity and P.A. are, respectively, much higher than and significantly misaligned with those of G1's observed isophotes.

As the shear strength is increased, the model galaxy's P.A. consistently rotates in the way that the misalignment

with G1's isophotes is reduced while the model galaxy's ellipticity remains relatively unchanged [specifically, it falls only moderately for small shear (e.g. $\gamma < 0.1$ for $\nu = 2$) but rises even higher for larger shear values]. For the isothermal galaxy model (and $\nu = 1.75$ model) considered above, for the galaxy to be aligned with the light (choosing P.A.$_{\text{light}} = 110°$), the required galaxy ellipticity and shear strength are $\epsilon = 0.90$ ($\epsilon = 0.82$) and $\gamma = 0.40$ (the same). Thus, the high ellipticity problem persists with the inclusion of a shear term. If one introduces an arbitrary shear rather than the above astrophysically motivated shear within single plane lensing framework, in other words if one allows the shear orientation to be arbitrary, it is possible to fit the data with likely galaxy parameters based on the observed light distributions. For the isothermal galaxy model (and $\nu = 1.75$ model) considered above, a galaxy with $\epsilon = 0.3$ and P.A. $= 110°$ can fit the data providing $\gamma = 0.47$ ($\gamma = 0.36$) and $\theta_\gamma = -28°$ ($\theta_\gamma = -26°$). However, as pointed out above, these shear orientations are not expected for single plane lensing.

To summarize the results of single plane lens modelling of B2114+022 A, D, for the model galaxy allowed to be misaligned with G1's light, the minimum required ellipticity is $\epsilon = 0.76$ ($\epsilon = 0.57$) for $\nu = 2$ ($\nu = 1.75$), while for the model galaxy aligned with G1's light, the model requires $\epsilon = 0.90$ ($\epsilon = 0.82$) as well as a shear of $\gamma = 0.40$ for $\nu = 2$ ($\nu = 1.75$). For this latter case of a likely mass position angle of G1, the required large shear strength and the required very flattened projected mass density of G1 are unrealistic. This failure of single plane lens models in explaining the simple lensing constraints of B2114+022 leads us to one of the following two possibilities: Either single plane lensing is not applicable to this system because G2's lensing effects are comparably important or the lensing hypothesis on components A and D is doubtful. However, the latter possibility cannot be justified unless one has applied the more accurate theory to the system, namely two plane lensing theory. Next we investigate two plane lens models of B2114+022.

3.2.2 Two Plane Lens Model

The formalism of two thin plane lensing was reviewed in section 2. Using this formalism and adopting the mass model of equation (12) for each of the two galaxies at their observed positions and redshifts, we calculate the theoretical deflection, magnification and time delays due to the two deflectors using a code employing Fourier expansion techniques (Chae, Khersonsky & Turnshek 1998), and then fit the observed positions and flux ratio of components A and D by varying model parameter values of the galaxies. For this problem, we are fortunate to have relatively high-quality optical data on the two galaxies. The redshifts and optical centres of the two galaxies are directly used to constrain the lens model. The observed light distributions (in terms of ellipticities and position angles) of the two galaxies can be used to test astrophysical plausibility of the model ellipticities and position angles. While the lower redshift galaxy G1's observed properties are intrinsic properties, the higher redshift galaxy G2's observed properties are modified (i.e. lensed) properties of G2 due to the potential of G1. The relatively small angular separation between the two observed galaxies ($d_{12} \approx 1.''30$, which corresponds to the impact parameter for light rays

---

[★] In single plane lensing, we assume that the two galaxies are projected onto a single plane. A choice on the redshift of the plane is irrelevant here since we do not know the source redshift. The lensing effect of G1 changes G2's apparent position relative to G1 primarily in the radial direction; it affects the position only slightly tangentially.

from the G2 centre at the lensing plane of G1) ensures that the lensing of G2 by G1 is significant. In particular, we expect a shift in the galaxy's optical centre, stretching of light ellipses approximately along the east-west line (i.e. perpendicularly to the line joining G1 and G2) and possibly additional distortions of the stretched ellipses beyond a certain radius (i.e. arc-like light shapes).

Solving two plane lensing involves solving the single plane lensing of the extended background source by the foreground deflector. Ultimately, the lensed light distribution of G2 can be derived by subtracting out G1's light distribution, and the resulting extended arc-like light distribution can be used as a lensing constraint on G1's potential. However, due to our present lack of a suitable means to quantitatively deal with this problem and limited quality of the presently available data for this purpose, in this paper we do not fit G2's light distribution but use it to qualitatively test astrophysical plausibility of the intrinsic ellipticity and position angle of the G2 mass model. We know *a posteriori* that for comparable masses of G1 and G2 for the observed geometric arrangement, the lensing effect of G1 leads to a net increase of G2's ellipticity by ≈ 0.2–0.3 along approximately east-west. This allows us to limit possible ranges of the ellipticity and position angle of G2's intrinsic light distribution (which can in turn provide some information on G2's mass distribution). Loosely speaking, an intrinsically elliptical G2 cannot be oriented along east-west since such a light distribution would become more elliptical than observed due to a net increase in the same direction caused by G1, and thus it should be roughly oriented along north-south. The intrinsic ellipticity of G2's light then depends on a stretching by G1 and the measured value of G2 image's ellipticity. For example, for a measured ellipticity of 0.1 and an amount of stretching of 0.25, the required G2's intrinsic ellipticity is 0.15 for a P.A. of zero.

For a given radial profile (ν) for each model galaxy, the mass distribution is determined by parameters Σ_0, ξ_c, ϵ and θ_0 [equation (12)]. However, since neither Σ_0 nor ξ_c is sensitive to the lensing properties of the model (other than a relationship between ξ_c and relative magnification of a theoretical image near the mass centre), we use an Einstein ring radius (ξ_E) which is directly related to the deflection scale of the model galaxy and insensitive to the choice of either ξ_c or Σ_0.[†] We use a ξ_E determined from

$$\frac{\xi_E^2}{\xi_c^2} = \frac{2\kappa_0}{3-\nu}\left[\left(1+\frac{\xi_E^2}{\xi_c^2}\right)^{\frac{3-\nu}{2}} - 1\right] \qquad (14)$$

for the mass model of equation (12). For a single-galaxy lens, parameter ξ_E is well constrained regardless of the choice of lens model parameters. For the two-galaxy model under consideration, the lensing effect is the combined effect due to the two deflectors. Thus, we do not expect individual Einstein ring radii of the galaxies to be well constrained for a two-galaxy lens system, while we may expect the 'sum' of them to be. A parameter controlling the relative size of two Einstein ring radii (or masses enclosed within them) is a fundamental parameter of interest in a two-galaxy system

---

[†] For a ξ_E, fixing either ξ_c or Σ_0 determines the other.

which we intend to constrain. In this study, we define a total Einstein ring radius $\xi_E^{\text{tot}} \equiv \xi_E^{(1)} + \xi_E^{(2)}$ and a parameter

$$f_2^R = \frac{\xi_E^{(2)}}{\xi_E^{\text{tot}}}, \qquad (15)$$

which controls the relative size of Einstein ring radii of the two galaxies. We also define a parameter

$$f_2^M = \frac{M_E^{(2)}}{M_E^{\text{tot}}}, \qquad (16)$$

where $M_E^{\text{tot}} = M_E^{(1)} + M_E^{(2)}$ and $M_E^{(i)}$ ($i = 1, 2$) are the masses enclosed within the Einstein ring radii of G1 and G2 respectively.

We first consider isothermal profiles $\nu^{(i)} = 2$ ($i = 1, 2$ where labels 1, 2 denote G1, G2 respectively hereafter). Out of the six remaining parameters of the two galaxies, some of the parameters are *a posteriori* trivial or confined within relatively small ranges. As was discussed above, we expect G2's mass distribution to be oriented approximately north-south. Remarkably, we find that in order to fit the data G2's P.A. ($\theta_0^{(2)}$) has to be approximately within a quadrant around north. We fix G2's P.A. at $\theta_0^{(2)} = +10°$ since at other angles the required ellipticity of G2 is higher and we do not expect a high intrinsic ellipticity for G2 (see the discussion above). As is always the case in lensing, an appropriately defined total mass (or, equivalently deflection scale) for lensing is expected to be well constrained. For the two-galaxy model under consideration, parameter ξ_E^{tot} is confined within a relatively small range. However, parameter f_2^R is not well constrained by (at least present) lensing constraints. We fix f_2^R for each model, and increment its value between 0.3 and 0.5 which were chosen *a posteriori*. We expect the position angle of G1's mass model ($\theta_0^{(1)}$) to be similar to that of G1's observed light distribution, i.e. $100° \lesssim \text{P.A.}_{\text{light}}^{(1)} \lesssim 110°$ for $0''.1 \lesssim r_{\text{max}} \lesssim 0''.5$ (Figure 3). We find, however, that the fitted value of $\theta_0^{(1)}$ for a large region of parameter space tends to be more north-south oriented than P.A.$_{\text{light}}^{(1)}$. We fix $\theta_0^{(1)}$ for each model and increment its value in the range between $100°$ and $150°$.

With the above prescriptions, we determine the other parameters (i.e., $\epsilon^{(1)}$, $\epsilon^{(2)}$ and ξ_E^{tot}) for each model by varying them simultaneously. In this way we calculate a grid of models covering realistic ranges of model parameters. Due to the small number of observational constraints, each model gives a perfect fit to the data. Parameters ξ_E^{tot} and $\theta_0^{(2)}$ being trivial, parameters of our primary interest are $\epsilon^{(1)}$, $\theta_0^{(1)}$, $\epsilon^{(2)}$ and f_2^R. We find that for most models in the grid $\epsilon^{(1)}$ is confined within a relatively small range of $0.3 \lesssim \epsilon^{(1)} \lesssim 0.4$. Thus, the required extraordinarily high ellipticity for G1 encountered in the single plane lens model (considered in section 3.2.1) is not necessary when G2's potential is included at its observed redshift. Correlations among the other three parameters $\theta_0^{(1)}$, f_2^R and $\epsilon^{(2)}$ can be found in Figure 4a which also shows the parameter f_2^M. An upper limit on f_2^R (equivalently f_2^M) for each $\theta_0^{(1)}$ is set by the requirement that any predicted image near G2's centre should be fainter than the observational flux limit on any unobserved image (i.e. 2.4% of component D flux density). Thus, G2 can only be somewhat less massive than G1 based on the two isothermal galaxies model. Combined with the observationally inferred luminosity ratio between the two galaxies of $L(\text{G2})/L(\text{G1})$
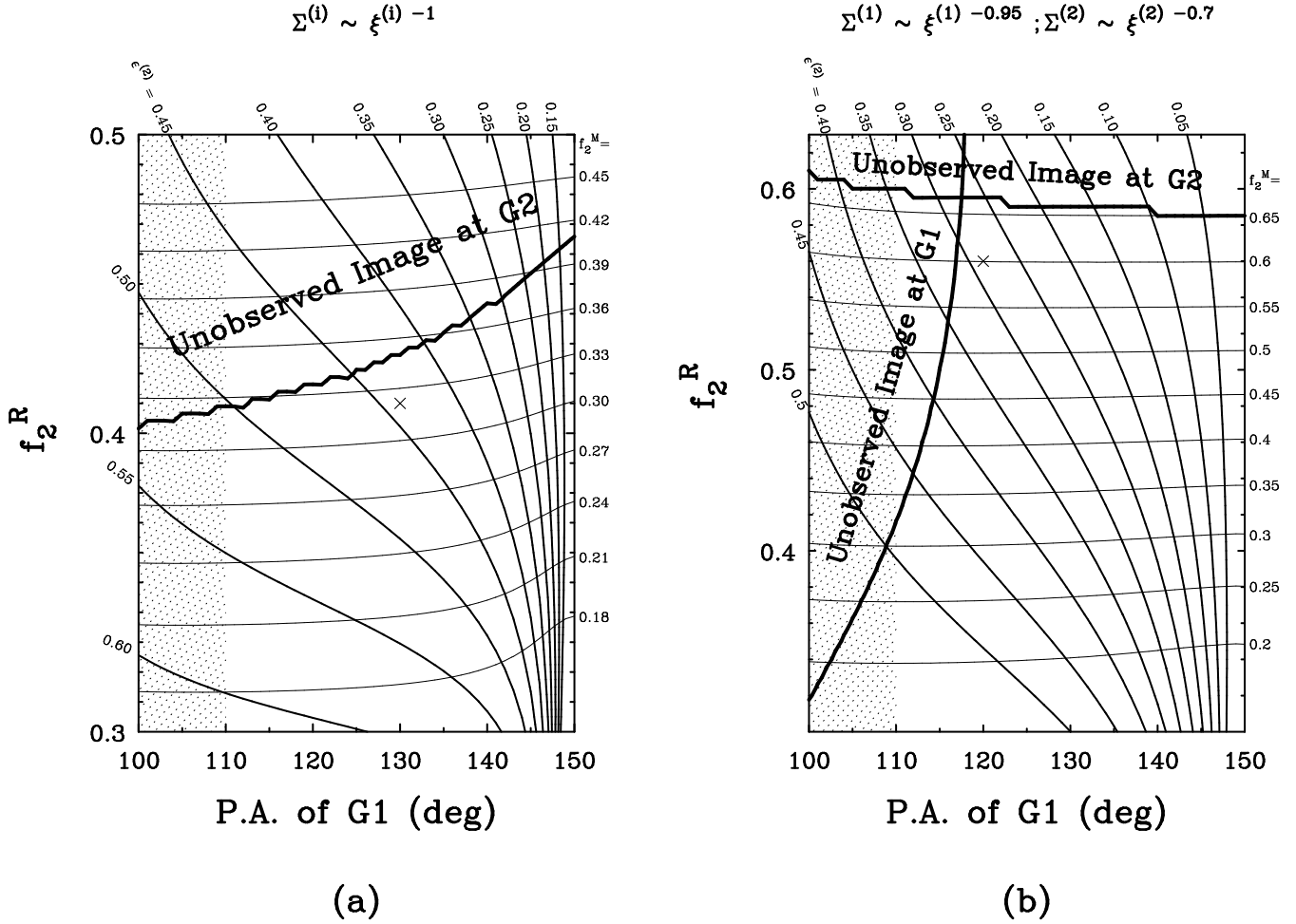
Figure 4. (a) Correlations among parameters $\theta_0^{(1)}$ (G1's P.A.), f_2^R [equation (15)] and $\epsilon^{(2)}$ (G2's ellipticity) for two isothermal galaxies model. Parameter f_2^M defined by equation (16) is also shown for a reference to the mass ratio between the two galaxies. The hatched region is the observed range of position angle. The parameter space above the thick solid line is ruled out due to predicted additional bright images near G2 that are not observed. A cross indicates an example model whose parameters and predictions are given in Table 2. (b) Similar correlations among the same parameters as in (a) for the mass profiles $\nu^{(1)} = 1.95$ and $\nu^{(2)} = 1.7$ for G1 and G2 respectively. Compared with the two isothermal mass profiles model in (a), for these shallower mass profiles the upper excluded region due to additional images near G2 is pushed upward while a region left of the thick vertical line is now excluded due to a predicted bright image near G1.

~ 2 (section 3.1.2), the upper limits on f_2^M (Figure 4a) would imply that the mass-to-light (M/L) ratio of G1 is higher than that of G2 at least by a factor of ~ 4. As a consequence of this relatively large implied mass of G1 in the isothermal galaxies model, the model predicts relatively large stretching and distortion of G2's light distribution. Table 2 gives parameters and predictions of an example two isothermal galaxies model marked by a cross in Figure 4a (Model 1). The ranges given in the table are only for models with $\epsilon^{(i)} < 0.5$ $(i = 1, 2)$ and $|\theta_0^{(1)} - \text{P.A.}_{\cdot\text{light}}^{(1)}| < 30°$ in the grid. Predicted lensing of G2's light distribution by G1 is shown in Figure 5: G1's lensing on G2 leads to a stretching of G2's light distribution by $\Delta\epsilon \approx +0.3$ approx-

imately along east-west. For an observed light ellipticity of $\epsilon_{\text{obs}}^{(2)} \approx 0.15$ (Figure 3), a stretching of $\Delta\epsilon \approx +0.3$ implies an intrinsic ellipticity of $\epsilon_{\text{int}}^{(2)} \approx -0.15$ along east-west (i.e. $\epsilon_{\text{int}}^{(2)} \approx +0.15$ along north-south). From the two isothermal galaxies model grid of Figure 4a, we find that the required mass ellipticity of G2 is much higher than the inferred intrinsic light ellipticity of G2, especially for models in which G1's light and mass are aligned (the hatched region in Figure 4a) [while the required mass ellipticity of G1 is similar to or slightly higher than the light ellipticity of G1]. This could be taken as a model-dependent evidence for a significantly flattened dark matter halo for G2, under the con-

Table 2. Example two-plane lens model parameters and predictions. For Model 1, both G1 and G2 have isothermal profiles, while for Model 2, G1 and G2 have different and shallower-than-isothermal profiles. The parameter values given are for the models marked by a cross in Figure 4a,b. The parameter ranges given in parentheses are for models with $\epsilon^{(i)} < 0.5$ ($i = 1, 2$) and $|\theta_0^{(1)} - \text{P.A.}_{\text{light}}^{(1)}| < 30°$.

Parameter	Description	Model 1	Model 2
ξ_E^{tot} (h_{60}^{-1} kpc)	Sum of Einstein radii of G1 & G2	7.11 (6.6–7.2)	6.85 (5.7–7.7)
f_2^R	See equation (15).	0.41 (0.33–0.44)	0.56 (< 0.6)
$\nu^{(1)}$	Radial index of G1	2	1.95
$\nu^{(2)}$	Radial index of G2	2	1.7
$\epsilon^{(1)}$	Ellipticity of G1	0.32 (0.30–0.44)	0.37 (0.14–0.5)
$\epsilon^{(2)}$	Ellipticity of G2	0.44 (0.32–0.5)	0.29 (0.09–0.5)
$\theta_0^{(1)}$ (deg)	P.A. of G1	130 (111–140)	120 (108–140)
$\theta_0^{(2)}$ (deg)	P.A. of G2	10	10
Prediction			
$\xi_c^{(1)}$ (h_{60}^{-1} kpc)	Core radius of G1	< 0.073	< 0.010
$\xi_c^{(2)}$ (h_{60}^{-1} kpc)	Core radius of G2	no limit	no limit
M_E^{tot} ($10^{11} M_\odot$)	Sum of Einstein masses of G1 & G2	1.92 (1.8–2.0)	1.70 (1.4–2.4)
f_2^M	See equation (16).	0.32 (0.19–0.38)	0.60 (< 0.67)
t_{AD} (h_{60}^{-1} days)	Time for A delaying D	86.3 (83.–89.)	66.4 (47.–81.)
$\mathcal{M}_A + \mathcal{M}_D$	Sum of magnifications for A & D	10.3 (8.8–11.)	16.6 (10.6–30.5)

dition that G2's radial mass profile is isothermal and G1's light and mass are aligned [this latter condition is likely to be valid (see above in section 3.2)]. Conversely, the required high ellipticity of G2 could be taken as an argument for a shallower-than-isothermal profile for G2, which we consider below. It is also worth emphasizing that the two isothermal galaxies model imply a large difference between M/L ratios of the two galaxies (at least by a factor of ~ 4; see above).

The relatively high ellipticity of G2 required in the two isothermal galaxies model can be significantly reduced by making the radial profile of G2 somewhat shallower than isothermal. In this case the required ellipticity for G1 of an isothermal profile slightly increases. However, this increase in G1's ellipticity can be avoided by making the radial profile of G1 slightly shallower than isothermal. Similarly to the case in the single plane lens model considered in section 3.2.1, for a significantly shallower-than-isothermal profile of G1 a theoretical image near G1's centre becomes brighter than the observational limit, insensitive to the core radius of G1. A model with $\nu^{(1)} = 1.95$ and $\nu^{(2)} = 1.7$ was calculated and relationships among parameters $\theta_0^{(1)}$, f_2^R and $\epsilon^{(2)}$ can be found in Figure 4b. In this model, parameter f_2^M [equation (16)] covers a wider range compared with the two isothermal galaxies model, including values implying G2 more massive than G1. In particular, within the upper limits of f_2^M, G2 could be twice as massive as G1 implying that both galaxies have similar M/L ratios. As Figure 4b shows, with the chosen radial profiles for the two galaxies, one can find a model in which model position angles and ellipticities for both G1 and G2 are not too different from those for the observed light distributions. The parameter values for such a model (marked by a cross in Figure 4b) are given in Table 2 (Model 2). Predicted lensing of G2's light distribution by G1 is shown in Figure 5. In this model the amount of predicted stretching for G2 is $\Delta\epsilon \approx 0.2$, which implies an intrinsic light ellipticity of $\epsilon_{\text{int}}^{(2)} \approx 0.05$ along north-south for $\epsilon_{\text{obs}}^{(2)} \approx 0.15$. Compared with the predictions of Model 1 (Figure 4a), Model 2 predicts somewhat weaker distortions. In

Model 2, the mass ellipticities are relatively low but slightly higher than their observed/inferred intrinsic light ellipticities and G1's mass distribution is misaligned with G1 light ellipses by only $\sim 10°$. The critical curves and caustics for this model are shown in Figure 6.

4   DISCUSSION AND FUTURE WORK

In this paper, we have tested and analysed in detail the simplest and observationally most consistent lensing hypothesis for the JVAS quadruple radio source B2114+022, namely that the two widest separated, observationally similar radio components A and D of B2114+022 are lensed images of a background radio source due to the two galaxies at different redshifts. Although we have tested other lensing scenarios (in which all the four components or three components A, B and D are lensed images of a background source) and find that they can be consistent with the geometry and radio flux density ratios, present independent evidence indicating that components B and C have different radio surface brightness distributions and radio spectra compared to components A and D did not justify detailed analyses of such scenarios. However, we will have to revisit those lensing scenarios in the future if new data and/or new interpretations of the present data warrant it.

Our study finds that the radio components A and D of B2114+022 can be successfully reproduced by astrophysically plausible two-plane models consistent with the observed properties of the galaxies. In particular, the unusual flux ratio, i.e. the image closer to the lensing galaxies being brighter, can be easily reproduced in our model. Short radio jets in the north of component A core and those in the south of component D core (see Figure 2 of A00) are also consistent with our lens model prediction; qualitatively, theoretical jets in the south of the radio core on the source plane can reproduce the jets, based upon our lens models. Global VLBI observations of these jets in the near future will reveal

## G2 Intrinsic   G2 Image: Model 1   G2 Image: Model 2
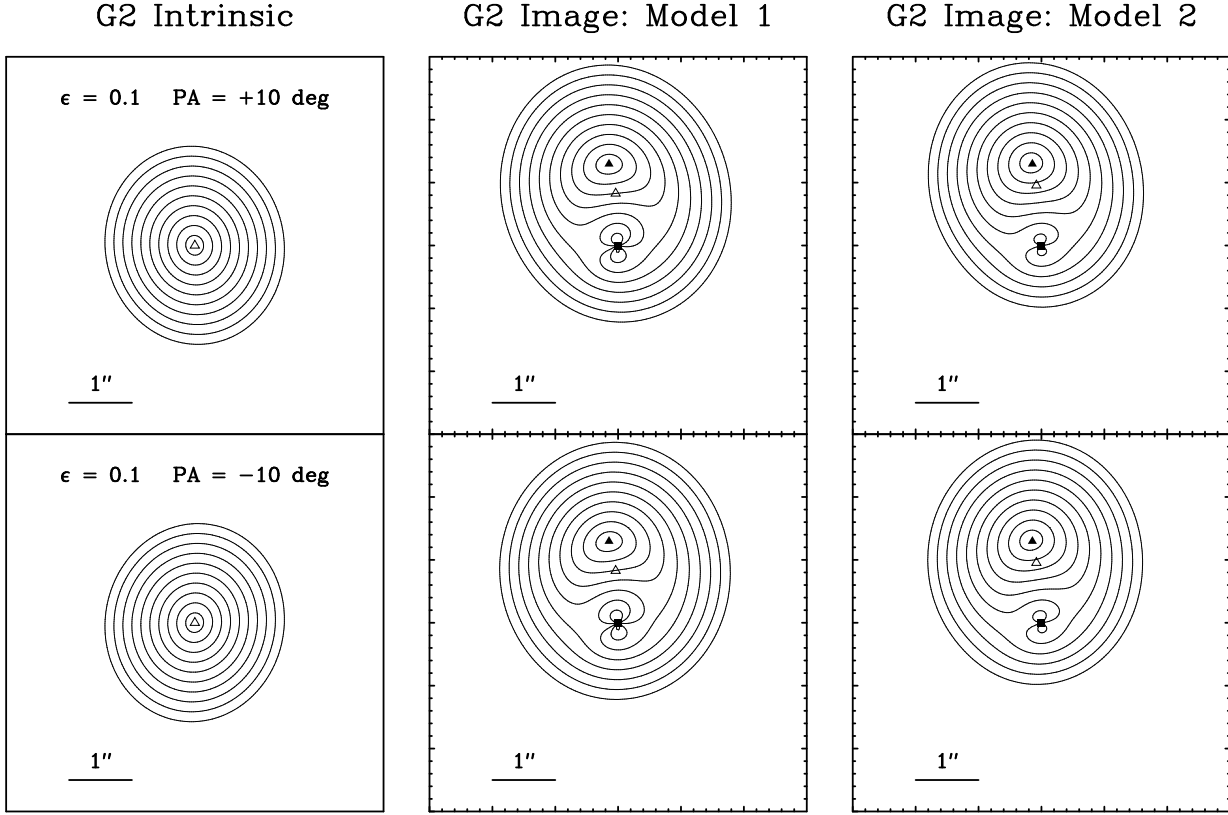
Figure 5. Predicted shift, stretching and distortion of the background galaxy's (G2) isophotes induced by the foreground galaxy (G1). An intrinsic G2's ellipticity of 0.1 for two position angles P.A. = +10° (aligned with the mass model P.A.) and P.A. = −10° are considered (left panels). The 10 ellipses correspond to semi-major axes of 1, 2, ..., 10 h_{60}^{-1}kpc at $z_2 = 0.5883$. Middle panels and right panels are predicted images for Model 1 and Model 2 (Table 2 and Figure 4) respectively. Notice that the inner several kpc regions of G2 have P.A.s nearly orthogonal to the intrinsic P.A.s in these models. The filled squares and triangles denote observed G1 and G2 positions while the open triangles denote the model-predicted intrinsic position of G2.

more detail and provide more stringent constraints on lens models for B2114+022. Since the optical counterparts of the radio sources appear to be extremely faint and are close to the two lensing galaxies (see section 3.1.1), it will be an observational challenge to obtain optical spectra of the four components to spectroscopically verify the lensing hypothesis. However, our realistic model grid (Figure 4) predicts a range of time delays from $\approx 50 - 90 \; h_{60}^{-1}$ days between the two components with component D leading component A. So if a future radio monitoring program could identify a correlated variability between these two components with a time delay, this would confirm the lensing hypothesis independently. A00 have found no significant variability for the radio sources to date.

Although there are at present only a small number of direct and indirect lensing constraints available for B2114+022, the unique geometric arrangement of the system and the D/A flux ratio appear to allow us to probe galaxies mass profiles in terms of radial power-law slope and core radius. Our study indicates that models adopting two isothermal mass profiles for the foreground (G1) and background (G2) galaxies potentially may not be a partic-

ularly good fit to some observed properties of B2114+022. They require a relatively high mass ellipticity ($\epsilon \sim 0.5$) for G2 while the inferred intrinsic light distribution is nearly round ($\epsilon \sim 0.1$). They also imply a much larger (at least by a factor of ~ 4) M/L ratio for G1 than for G2, which could pose a potential problem for the model.[‡] These potentially problematic features of the two isothermal galaxies model, as we have shown in section 3.2.2, can be avoided if a shallower-than-isothermal profile is adopted for G2. However, definitive bounds could not be put on G2's radial slope from lensing analyses of this system mainly because image splitting occurs with respect to G1's centre than G2's centre [although the undeflected source position can be closer to G2's centre than G1's centre (see Figure 6)] and as a result G2's mass profile is less sensitive to lensing properties. Likewise, no bound on the core radius of G2 can be put us-

[‡] The spectra of the two galaxies show that G1 is a post-starburst elliptical, which A00 classify as "E + A" type, while G2 is a normal elliptical. Potential extra light and dust in G1 complicate using mass ratios of the galaxies to test lens models.
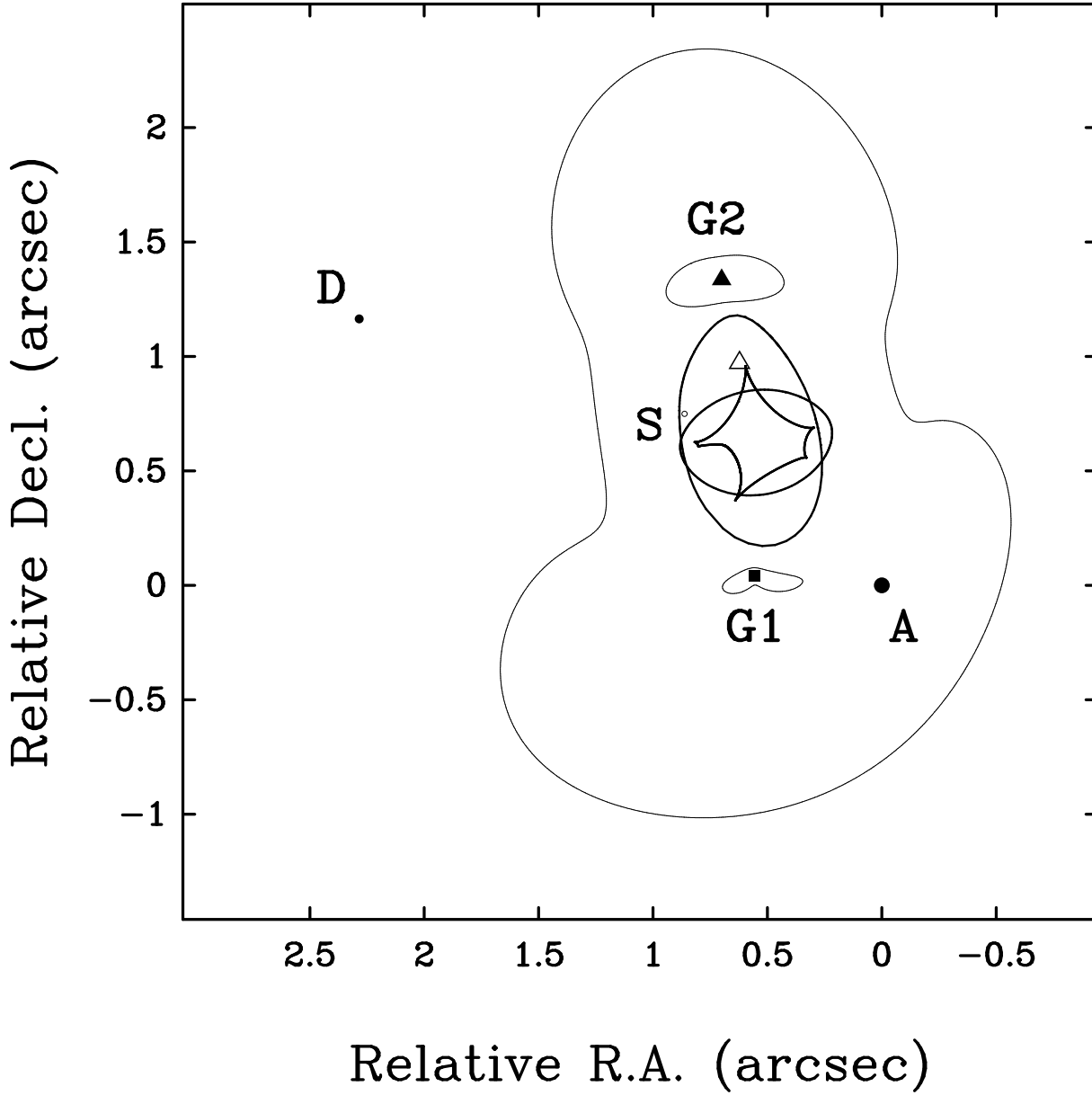
Figure 6. An example lens model for radio cores A and D (Model 2; see Table 2, Figure 4b and Figure 5). The two lensing galaxies are indicated by filled square and triangle for G1 and G2, respectively. The 'true' position of the background galaxy is indicated by an open triangle predicted by the model. The predicted source position of the images is indicated by a small open circle marked by 'S'. The caustics and critical curves for the model are drawn with thick and thin solid lines, respectively.

ing a theoretical image closest to G2 which may or may not form. Instead, whether bright theoretical images near G2 can form or not is controlled by a mass ratio between the two galaxies as illustrated in Figure 4. Specifically, beyond the upper bound on f_2^M, the smaller ellipse-like caustic in Figure 6 grows to enclose the source, allowing two additional images near G2 to form.

Unlike G2's mass profile, however, definitive limits on G1's radial power-law slope ($\nu^{(1)}$) and $\nu^{(1)}$-dependent core radius can be put using a theoretical image forming near

G1's centre. As illustrated in Figure 4b, for a relatively shallow radial profile of G1 a region of parameter space becomes excluded due to a predicted bright image near G1 whose brightness is insensitive to the core radius. As G1's profile gets shallower, this excluded region grows and a profile shallower than $\nu^{(1)} \approx 1.90$ is virtually excluded for G1 since such a profile does not allow a realistic P.A. for G1. In addition to this definitive lower limit on G1's radial slope, a less strong but likely upper limit on G1's radial slope is suggested from our study, namely that a profile significantly

steeper than isothermal is not very likely since those profiles require mass ellipticities much higher than observed light ellipticities. Thus, a most likely radial power-law slope for G1 is a relatively shallow profile just over the lower limit. It is remarkable that relatively strong bounds can be put on a radial power-law slope of G1 with only a few number of lensing constraints available for B2114+022. For models outside the excluded parameter space regions (Figure 4), upper limits can be put on the core radius of G1 (see Table 2). With more strong lensing constraints provided by Global VLBI observations of the radio jets of B2114+022 A, D in the near future, this system offers a good possibility of determining the mass profile of G1 either using a simple model such as equation (12) or a more realistic model such as a two-component model simulating G1's luminous and dark mass components. We plan to address this in the future.

One striking natural consequence of a two-plane lens system (or, any system consisting of two close galaxies with different redshifts) that we draw attention to in this paper is that the background galaxy's light distribution is substantially modified by the foreground galaxy. The lensing effects are intermediate between weak lensing and strong lensing and include apparent shift of the galaxy position, changes of position angle and ellipticity, and distortions of isophotes generating arc-like isophotes for outer parts of the optical galaxy. While modifications of position angle and ellipticity are not observationally identifiable lensed features (since intrinsic position angle and ellipticity are not measurable), distorted arc-like isophotes are potentially observationally identifiable lensed features since they are unique to lensing. Predictions on arc-like isophotes depend on the mass ratio between the two galaxies (Figure 5). It will be important to obtain deeper HST images to test these predictions. Multi-colour images may be particularly useful since the foreground and background galaxies have different colours, and therefore it may be easier to identify systematic features in a colour map. Once the predicted lensed features could be measured in the future, these would provide strong constraints on the potential of the foreground galaxy.

Although only one two-plane lens candidate has been discovered so far, we expect many such cases to be discovered in the future. In particular, NGST and SKA will play crucial roles in identifying many two-plane lens systems in the optical (Barkana & Loeb 2000) and radio respectively. The prediction that 1–10 per cent of lenses may be two-plane lenses by Kochanek & Apostolakis (1988) is based on simple spherical lenses, it would be important to revisit the problem using more realistic lens models; we plan to address this question in a further work, with particular emphasis on how this fraction depends on cosmologies.

This study shows that the caustics and critical curves of two elliptical deflectors at different redshifts are extremely complicated (see Figure 6); these caustics include regions that can produce 7 or 9 images (with the central image strongly demagnified), similar to binary galaxies in single-plane lensing (Keeton, Mao & Witt 2000). The effects of additional images and moderate changes in isophotal shapes can potentially provide strong constraints on lens model parameters and perhaps cosmological parameters as well. Some of these effects were illustrated in this paper. In particular, the effects of additional images were used to put model-dependent limits on the mass ratio of the two galaxies (see Figure 4) and to limit the allowed range of the radial power-law slope of the foreground galaxy. This can be understood as follows. In the complicated caustic structure of the two plane lens (see Figure 6), the caustics close to the source are more sensitive to the change of some model parameters than in a simpler caustic structure lens. An idealized example further illustrates the potential power of two plane lenses as astrophysical tools. If we have two perfectly aligned galaxies at different redshifts lensing a distant source, the aligned background source will be imaged into two Einstein rings while the background galaxy is imaged into a third ring. If we model the lensing galaxies as singular isothermal spheres, then there are only two velocity dispersions that parameterize the lenses, while we have three Einstein ring size constraints. The one extra constraint can then be used to constrain other parameters such as cosmology. It will be very interesting to see in the near future whether two-plane lenses can be a robust tool for cosmological studies.

REFERENCES

Arnaboldi M., Cappaccioli M., Cappellaro E., Held E. V., Sparke L., 1993, A&A, 267, 21
Augusto P., et al., 2000, MNRAS, submitted (A00)
Barkana R., Loeb A., 2000, ApJ, 531, 613
Blandford R., Narayan R., 1986, ApJ, 310, 568
Browne I. W. A., 2000, in Gravitational Lensing: Recent Progress and Future Goals, ASP conference series, eds. T. G. Brainerd & C. S. Kochanek, in press
Buote D. A., Canizares C. R., 1997, in Galactic Halos: A UC Santa Cruz Workshop, ASP Conference series Vol. 136, ed. D. Zaritsky
Chae K.-H., Khersonsky V. K., Turnshek D. A., 1998, ApJ, 506, 80
Erdl H., Schneider P., 1993, A&A, 268, 453
Keeton C. R., Kochanek C. S., Falco E. E., 1998, ApJ, 509, 561
Keeton C. R., Kochanek C. S., Seljak U., 1997, ApJ, 482, 604
Keeton C. R., Mao S., Witt H. J., 2000, ApJ, 537, 697
Kochanek C.S., Apostolakis J., 1988, MNRAS, 235, 1073
Kovner I., 1987, ApJ, 316, 52
Norbury M., et al., 2000, MNRAS, submitted
Sackett P. D., 1999, in Galaxy Dynamics, ASP Conference series Vol. 182, eds. D. R. Merritt, M. Valluri and J. A. Sellwood
Sackett P. D., Rix H.-W., Jarvis B. J., Freeman K. C., 1994, ApJ, 436, 629
Sackett P. D., Pogge R. W., 1995, in Dark Matter, AIP Conference series Vol. 336, eds. S. S. Holt & C. L. Bennett
Schneider P., Ehlers J., Falco E.E., 1992, Gravitational Lenses (New York: Springer-Verlag)
Seitz S., Schneider P., 1992, A&A, 265, 1

This paper has been produced using the Royal Astronomical Society/Blackwell Science LaTeX style file.